PNAS
www.pnas.org

Supplementary Information for

High-performance All-Solid-State Batteries Enabled by Salt Bonding to Perovskite in Poly(ethylene oxide)

Henghui Xu[a,b], Po-Hsiu Chien[c,d], Jianjian Shi[a,b], Yutao Li[a,b,1], Nan Wu[a,b], Yuanyue Liu[a,b], Yan-Yan Hu[c,d], and John B. Goodenough[a,b,1]

[a]Materials Science and Engineering Program, The University of Texas at Austin, Austin, TX 78712; [b]Texas Materials Institute, The University of Texas at Austin, Austin, TX 78712; [c]Department of Chemistry and Biochemistry, Florida State University, Tallahassee, FL 32306; [d]Center of Interdisciplinary Magnetic Resonance, National High Magnetic Field Laboratory, Tallahassee, FL 32310

Yutao Li and John B. Goodenough
Email: lytthu@utexas.edu; jgoodenough@mail.utexas.edu

This PDF file includes:

www.pnas.org/cgi/doi/10.1073/pnas.1907507116

Supplementary Information Text

Experimental Section

Preparation of perovskite $Li_{3/8}Sr_{7/16}Ta_{3/4}Zr_{1/4}O_3$

$Li_{3/8}Sr_{7/16}Ta_{3/4}Zr_{1/4}O_3$ (LSTZ) was prepared by a solid-state reaction. Stoichiometric amounts of Li_2CO_3, $SrCO_3$, Ta_2O_5, and ZrO_2 were ground and heated at 900 ºC for 6 h, then the collected powder was ground again, pressed into a pellet, and fired at 1300 ºC for 10 h in air. The obtained $Li_{3/8}Sr_{7/16}Ta_{3/4}Zr_{1/4}O_3$ pellet was polished for Li^+ conductivity testing, and ball-milled into powder for filler use in the composite polymer electrolyte membrane.

Preparation of the composite polymer electrolyte membrane

PEO (Mw ~600,000) and Lithium bis(trifluoromethanesulfonyl)imide (LiTFSI) were first dissolved in acetonitrile at 60 ºC with an EO/Li mole ratio of 10. LSTZ powder was then added into the PEO/LiTFSI solution for stirring with a LSTZ weight percentage of 10, 20, 30, 50 wt.%. The PEO/LiTFSI/LSTZ suspension was mixed over-night before being poured in a polytetrafluoroethylene dish, dried in a vacuum oven at 50 ºC for 24 h to obtain the PEO/LSTZ membrane. The membranes were transferred to glove box and stored for use.

Symmetric Li|PEO/LSTZ|Li cell assembly

A PEO/LSTZ membrane was sandwiched between two identical lithium discs; the Li|PEO/LSTZ|/Li was pressed and sealed in a 2032 coin cell for testing. The plating/stripping curves were collected with a Land CT2001A battery-test system.

Solid-state Li|PEO/LSTZ|$LiFePO_4$ and Li|PEO/LSTZ|$LiNi_{0.8}Mn_{0.1}Co_{0.1}O_2$ batteries

Solid-state batteries were assembled with a Li anode, a PEO/LSTZ electrolyte membrane, and a $LiFePO_4$ (LFP) or $LiNi_{0.8}Mn_{0.1}Co_{0.1}O_2$ (NMC) cathode in an Ar-filled glove box. The stacked electrolytes and electrodes were then pressed to ensure a close contact before sealing in a coin cell. The LFP cathode was prepared by mixing LFP powder, carbon black, and PEO/LiTFSI in a weight ratio of 60:10:30 in acetonitrile. The obtained viscous slurry was then coated on a carbon-coated Al foil, and dried at 50 ºC overnight in vacuum to produce finally the cathode with an LFP mass loading of 3.5 mg cm^{-2}. For the preparation of the high-voltage cathode, NMC powder, carbon black, and PVDF/LiTFSI were mixed in a weight ratio of 80:10:10 in dimethylformamide solvent.

Electrochemical measurements

An Li-blocking electrode was prepared by sputtering Au on the LSTZ pellet surface for the Li-ion conductivity measurement of the sintered LSTZ pellet. For the PEO/LSTZ membrane, the ionic conductivity was tested via a symmetric SS|PEO/LSTZ|SS (SS = stainless steel) cell and evaluated during the temperatures from 25 to 80 ºC. The conductivity was calculated based on the surface area and the thickness of the pellet or the composite membrane. The Li-ion transference number (t_{Li+}) of PEO/LSTZ was measured in a symmetric Li cell with a DC polarization of 10 mV. The lithium ion transference number (t_{Li+}) was calculated with the equation:

$$t_{Li+} = \frac{I_s(\Delta V - I_0 R_0)}{I_0(\Delta V - I_s R_s)}$$

where the I_0 and I_s are the initial and steady-state currents, ΔV is the potential applied across the cell. R_0 and R_s represent the charge-transfer resistance before and after the polarization of the symmetric cell, respectively.

Linear sweep voltammetry was conducted with Li|PEO/LSTZ|SS coin cells at 45 ºC. EIS measurements were conducted on an Auto Lab workstation with an AC amplitude of 10 mV and a frequency range from 1 MHz to 0.1 Hz. Galvanostatic charge/discharge of the solid-state batteries were performed at different current densities at 45 ºC on a Land CT2001A battery-test system.

Materials characterization

The crystalline phases of the LSTZ pellet, PEO/LiTFSI, and PEO/LSTZ membranes were investigated by X-ray diffraction (XRD) analysis with a Rigaku MiniFlex 600 instrument. The morphology of the PEO-LSTZ membrane was characterized by SEM (FEI Quanta 650) coupled with an energy-dispersive microscopy EDX spectrometer. XPS measurements were performed to analyze the surface chemical states of the pristine and cycled PEO/LSTZ membrane on an Axis Ultra DLD spectrometer (Kratos). A Time-of-flight secondary ion mass spectroscopy (TOF-SIMS) instrument (IONTOF GmbH, Germany 2010) was used to collect the depth profiling and chemical analysis data of the PEO/LSTZ membrane. All the data were recorded under ultra-high vacuum at a pressure of 10^{-9} Torr. The detected secondary ions possessed a mass resolution of > 5,000 in a negative model. During depth profiling, a 500 eV Cs^+ (negative) ion beam was raster scanned typically over the cycled electrodes. A 20 ns pulsed Bi^+ ion beam (30 keV ion energy, 3.8 pA measured current) set in a high current mode was employed for depth profiling or high lateral resolution mapping (< 200 nm) analysis. All the pristine and cycles PEO-LSTZ samples tested for XPS and TOF-SIMS analysis were transferred in a home-made air-free capsule (U.S. Pattern Application Serial No. 14/445650) between the glovebox and equipment.

All solid-state magic-angle spinning (MAS) ^{6,7}Li NMR characterizations are performed with a 2.5-mm HXY Bruker probe under a spinning rate of 25 kHz. The operating Larmor frequencies of ^{6}Li and ^{7}Li are 73.6 MHz and 194.4 MHz, respectively. Both ^{6}Li and ^{7}Li NMR spectra were acquired with a single-pulse sequence. For ^{7}Li NMR, a solid 90º pulse length of 3.35 μs and a recycle delay of 2 s was used. For ^{6}Li NMR, the solid 90º pulse length was 4.75 μs and the recycle delay was 20 s. ^{6,7}Li NMR chemical shift was calibrated with an external reference of $LiCl_{(s)}$ at −1.1 ppm.

DFT Computation Details

DFT calculations were performed with the Vienna Ab-initio Simulation Package (VASP) (1, 2) having a PAW pseudopotential (3), Perdew-Burke-Ernzerhosf (PBE) exchange-correlation functional (4), and a kinetic energy cutoff of 400 eV for the plane-wave expansion. The perovskite (001) surface is modelled by a slab, as shown in Fig. S5. We used the 3 × 3 × 1 Monkhorst Pack k-points (5), and a vacuum layer of ~15 Å perpendicular to the slab. All atomic positions were fully relaxed until the final force on each atom was less than 0.01 eV/Å.

The adsorption energies of the LiTFSI and Li in LiTFSI were calculated as

$$E_{ads}\,(\text{LiTFSI}) = E(\text{sub}) + E(\text{LiTFSI}) - E(\text{sub} + \text{LiTFSI})) \quad (1)$$

$$E_{ads}\,(\text{Li}) = E(\text{sub} + \text{TFSI}) + E(\text{Li}_{atom}) - E(\text{sub} + \text{LiTFSI}) \quad (2)$$

$$E_{ads}\,(\text{Li}) = E(\text{TFSI}) + E(\text{Li}_{atom}) - E(\text{LiTFSI}) \quad (3)$$

where E(sub + LiTFSI) and E(sub) are total energies of the perovskite (001) surfaces with and without LiTFSI, respectively. E (sub + TFSI) are total energies of the perovskite (001) with TFSI. $E(Li_{atom})$ is the reference energy of Li atom, which can be chosen as the energy of bulk metal (this reference energy is canceled when comparing the adsorption energy.

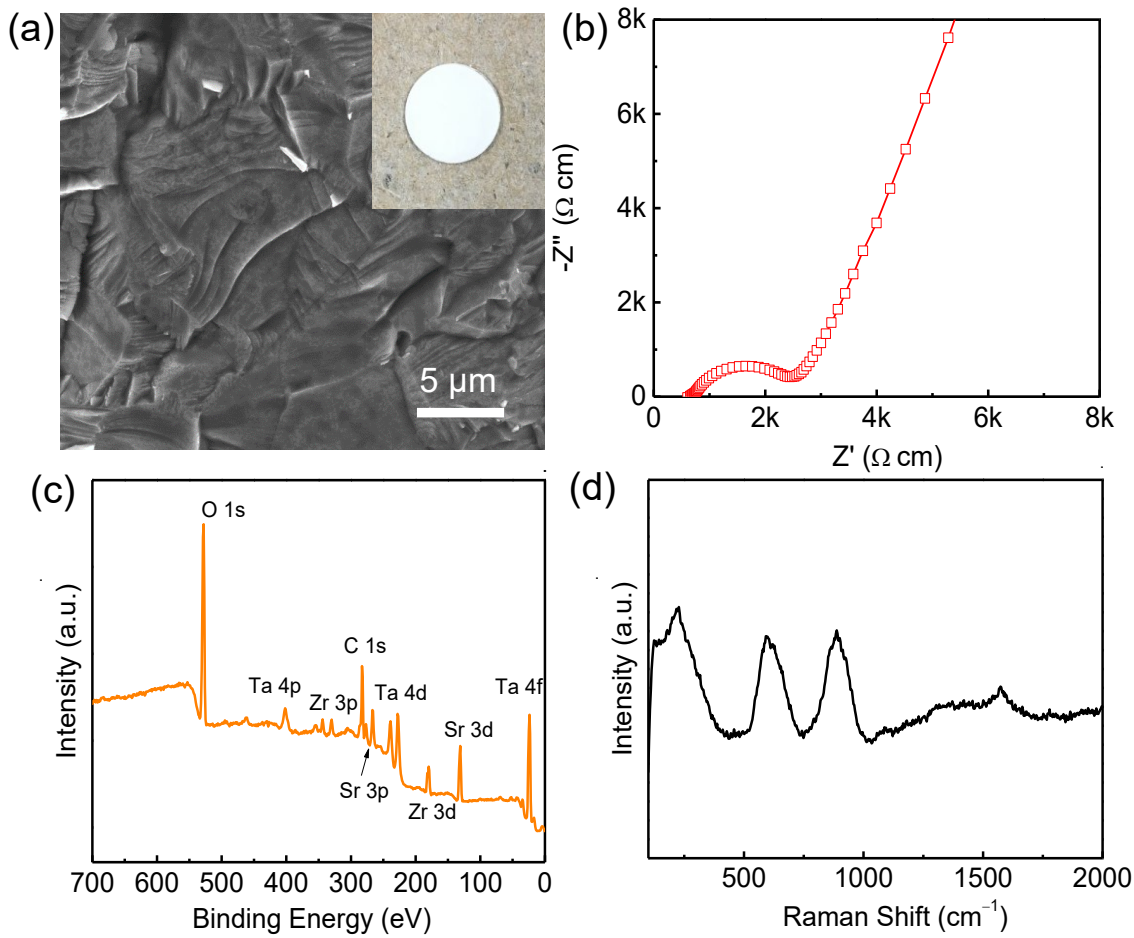

Fig. S1. (a) SEM image, (b) electrochemical impedance plot, (c) XPS survey spectrum, and (d) Raman spectrum of the LSTZ pellet. The EIS data in (b) is fitted with an equivalent circuit (R_{bulk}//(R_{gb}CPE)//CPE).

The pellet was very dense, and almost no grain boundaries were seen from Fig. S1a. The transcrystalline rupture showed very strong bonding between the grains. As a result, the Li^+ could transport rapidly without barriers of the grain boundaries. LSTZ has a high bulk Li^+ conductivity of 1.2×10^{-3} S cm^{-1} at room temperature (Fig. S1b). An XPS survey spectrum (Fig. S1c) reveals the presence of only Sr, Ta, Zr, and O elements in the LSTZ powder. Owing to the stability of LSTZ in moist air, there is no detected Li-insulating Li_2CO_3 on the surface of LSTZ (Figure S1d).

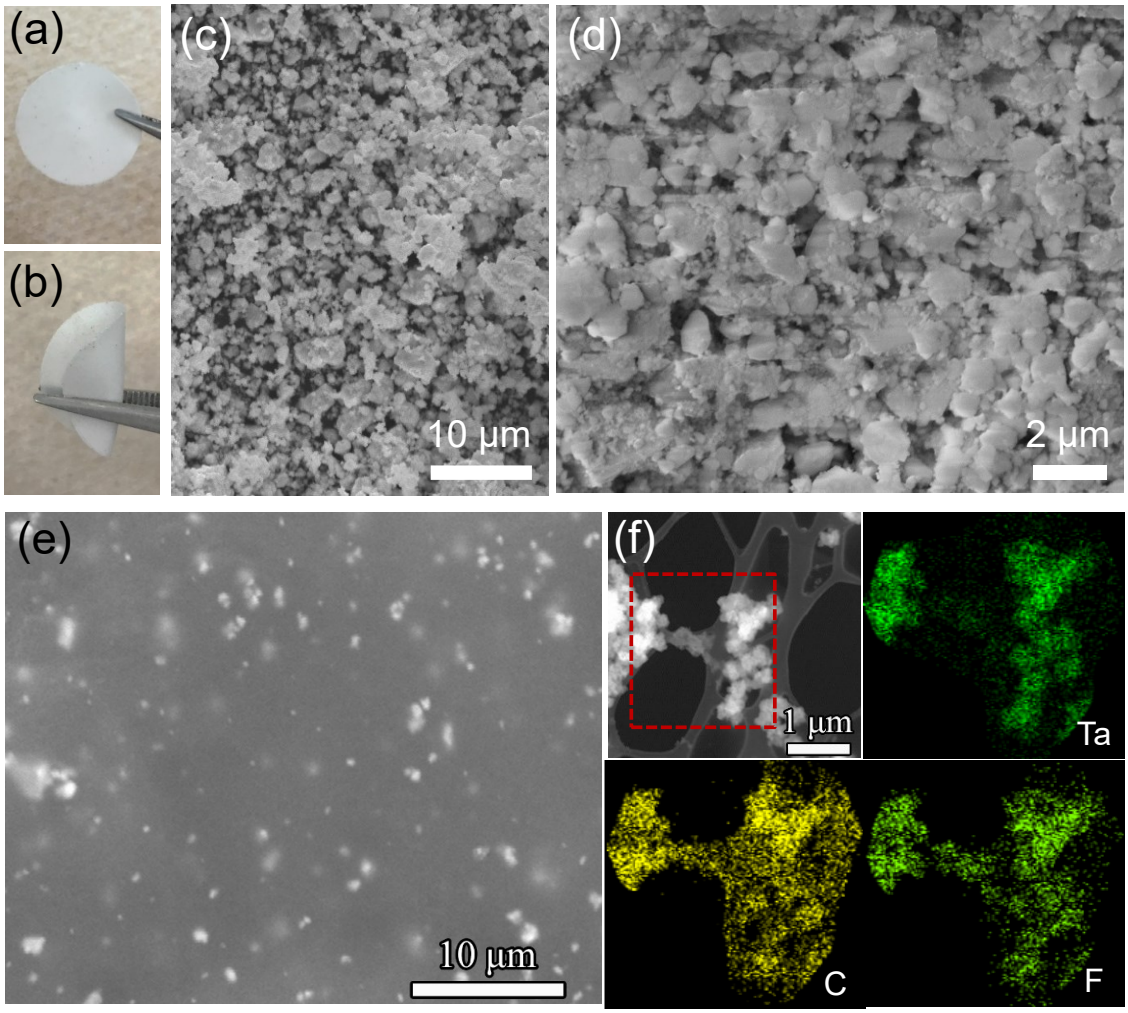

Fig. S2. (a, b) digital images of the as-preprared the PEO/LSTZ membrane. (c, d) SEM images of the ball-milled LSTZ powders. (e) SEM image of the PEO/LSTZ membrane. (f) Elemental mapping of Ta, C, and F in PEO/LSTZ acquired by a transmission electron microscope.

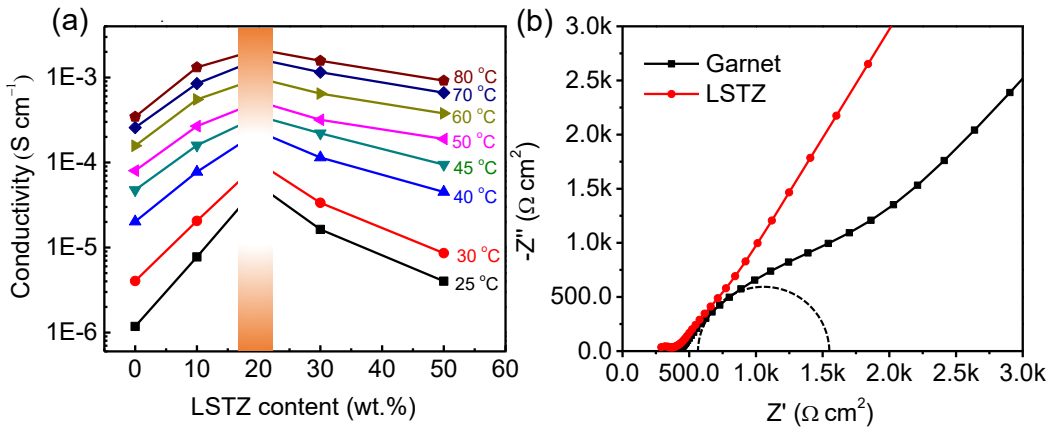

Fig. S3. (a) Ionic conductivity of PEO/LSTZ membranes with various LSTZ weight percentages of 0, 10, 20, 30, 50 wt% at different temperatures. (b) Comparative impendence of ss|PEO/LiTFSI|garnet|PEO/LiTFSI|ss cell and ss|PEO/LiTFSI|LSTZ|PEO/LiTFSI|ss.

Fig. S3b shows the interfacial impedance between PEO/LiTFSI membrane and LSTZ is only 75 Ω cm^2, much lower than that of garnet (~ 600 Ω cm^2). Although LSTZ and garnet have a similar high bulk conductivity, it is much easier for Li ions to transport from LSTZ to PEO/LiTFSI than from garnet to PEO/LiTFSI.

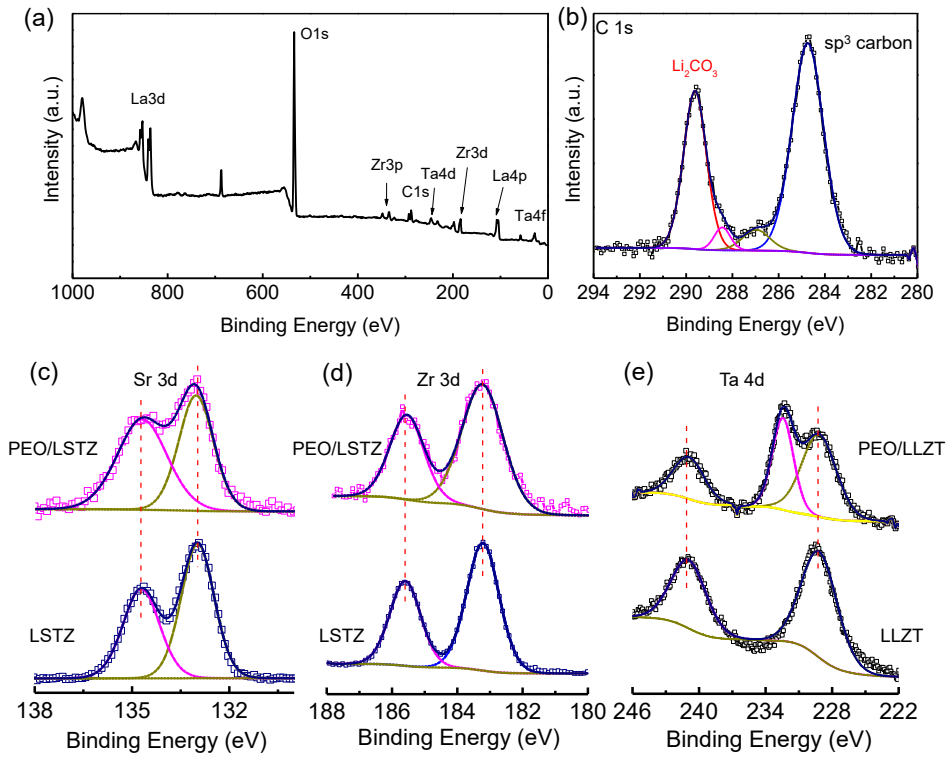

Fig. S4. (a) Survey and (b) C 1s high-resolution XPS spectra of Ta-doped $Li_{6.5}La_3Zr_{1.5}Ta_{0.5}O_{12}$ (LLZT), which show that Li_2CO_3 was coated on the surface of LLZT. High-resolution XPS spectra of (c) Sr 3d and (d) Zr 3d for LSTZ and PEO/LSTZ composite; neither the Sr nor Zr shows any obvious binder energy shift. (e) High-resolution Ta 4d XPS spectra of LLZT and PEO/LLZT composite.

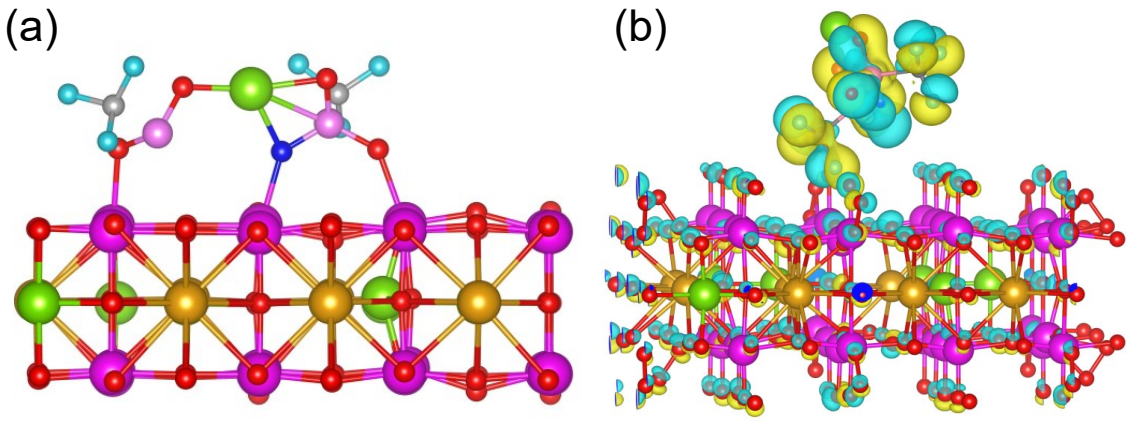

Fig. S5. (a) The crystallographic structure of LiTFSI adsorbed on the surface of Ta-terminated perovskite (001). (b) Differential charge density of the adsorbed LiTFSI on the O-terminated (001) surface of the perovskite LSTZ with one oxygen vacancy. Olive and blue colors represent increase and decrease of electronic distribution density, respectively. The isovalue is 0.034 e/Bohr3.

Ta-terminated perovskite (001) surface (Fig. S5a) was first considered as a stable substrate to adsorb the LiTFSI, but it would decompose TFSI and then become O terminated. Therefore, O-terminated perovskite (001) was deemed as a stable and favorable substrate.

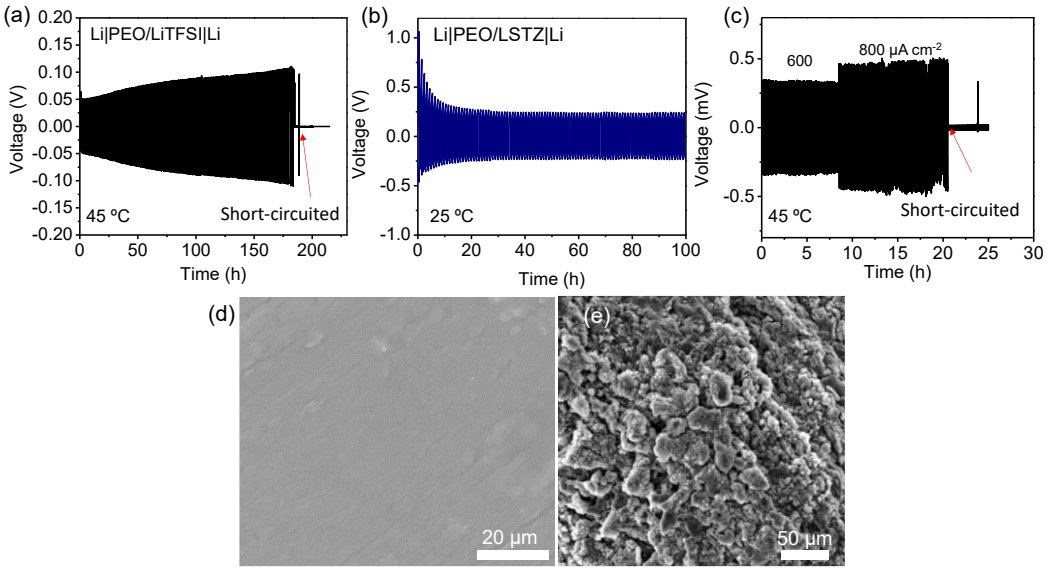

Fig. S6. (a) Voltage-time profile of Li|PEO/LiTFSI|Li symmetric cell cycled at 100 μA cm^{-2} and 45 ºC. Voltage-time profile of a Li|PEO/LSTZ|Li symmetric cell cycled at (b) 25 ºC (100 μA cm^{-2}) and (c) 45 ºC (600 and 800 μA cm^{-2}). SEM image of (d) a pristine lithium surface and (e) a Li surface collected from the Li|PEO/LiTFSI|Li symmetric cell after cycling at 100 μA cm^{-2} at 45 ºC.

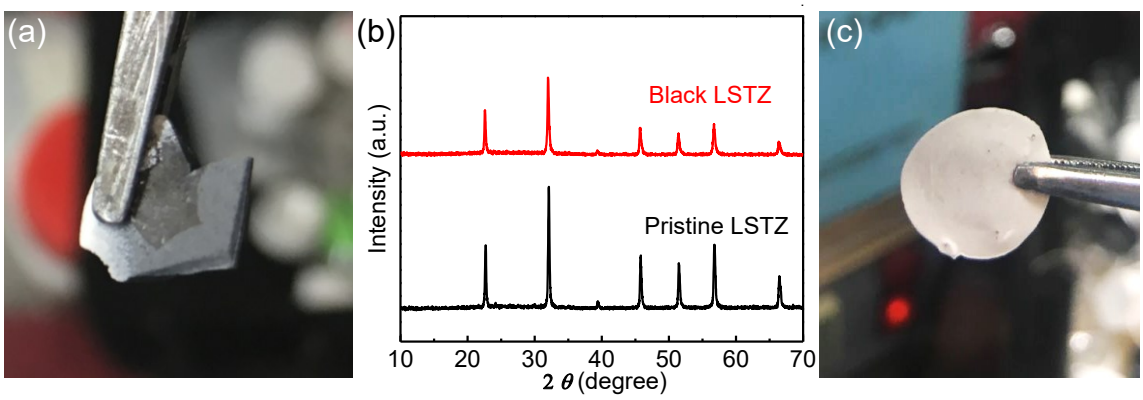

Fig. S7. (a) LSTZ pellet after contacting with Li metal. (b) Comparative XRD patterns of pristine LSTZ and black LSTZ pellets. (c) PEO/LSTZ membrane retrieved from cycled symmetric lithium cell.

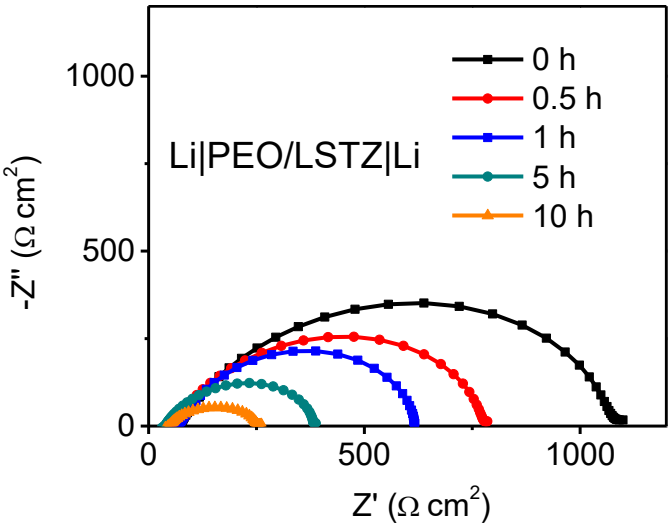

Fig. S8. A time-resolved EIS spectra of the Li|PEO/LSTZ|Li symmetric cell measured at OCV without cycling at 45 ºC.

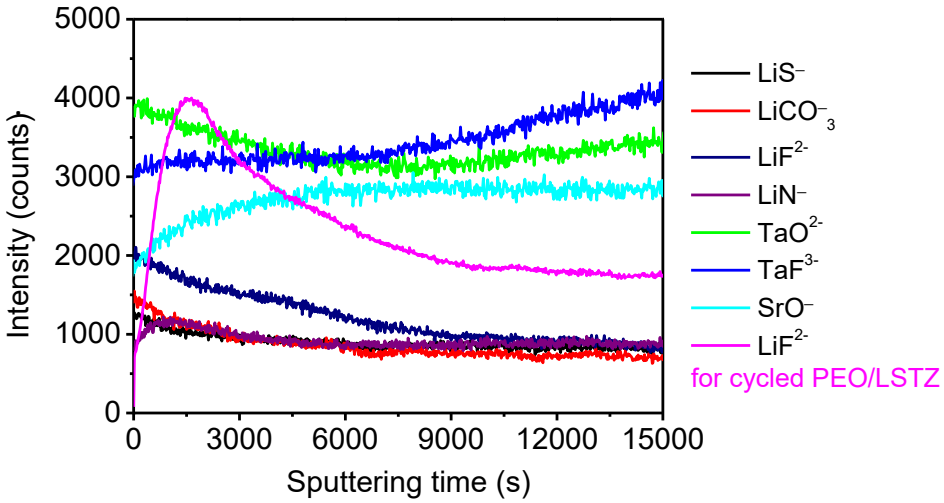

Fig. S9. Depth profile of the pristine PEO/LSTZ membrane; the LiF^{2-} signal (pink curve) from the cycled PEO/LSTZ was put here for comparison

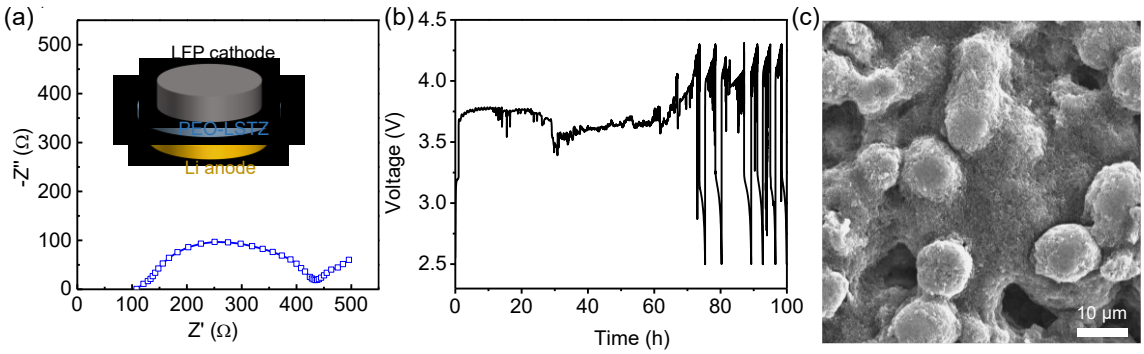

Fig. S10. (a) EIS of the solid-state LFP|PEO/LSTZ|Li cell tested at 45 ºC. (b) Voltage-time profile of NMC|PEO/LSTZ|Li solid-state batteries with PEO as the binder in the NMC cathode. (c) SEM image of the NMC cathode. NMC particles were uniformly covered by a PVDF binder. The PVDF can isolate the NMC particles and PEO/LSTZ electrolyte membrane, and thus prevent the PEO form being decomposed by the high-voltage NMC cathode.

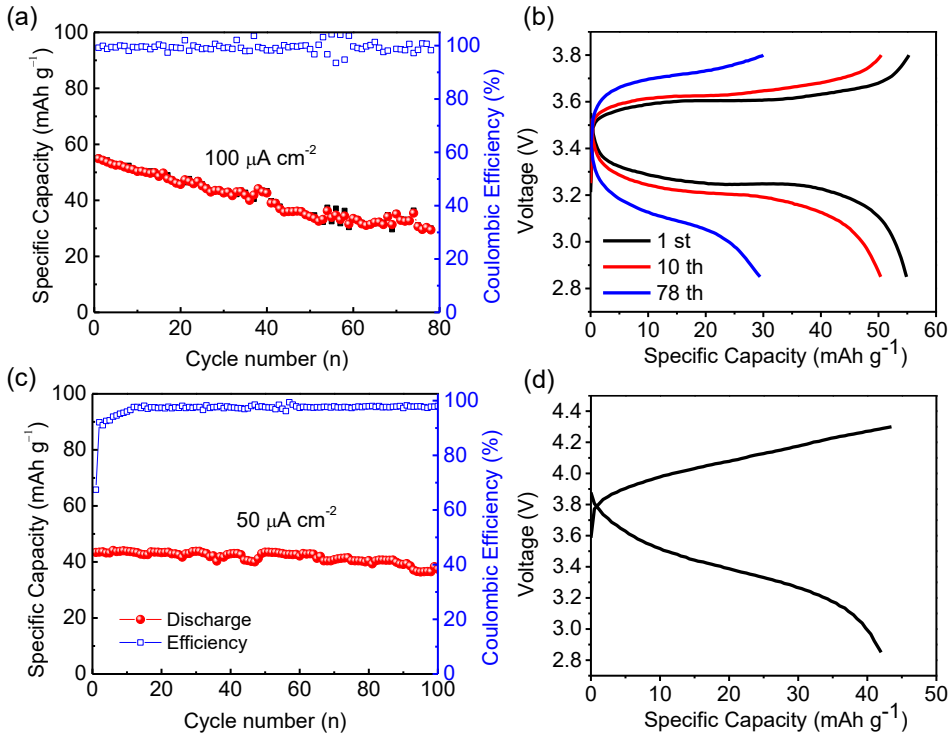

Fig. S11. Cycling performances and charge-discharge curves of (a, b) LFP|PEO/LSTZ|Li and (c, d) NMC|PEO/LSTZ|Li all-solid-state batteries measured at 25 ºC.

References

1. Kresse G Hafner J (1993) Ab initio molecular dynamics for liquid metals. *Physical Review B* 47(1):558-561.
2. Kresse G Furthmüller J (1996) Efficient iterative schemes for ab initio total-energy calculations using a plane-wave basis set. *Physical Review B* 54(16):11169-11186.
3. Kresse G Joubert D (1999) From ultrasoft pseudopotentials to the projector augmented-wave method. *Physical Review B* 59(3):1758-1775.
4. Perdew JP, Burke K, Ernzerhof M (1996) Generalized Gradient Approximation Made Simple. *Physical Review Letters* 77(18):3865-3868.
5. Monkhorst HJ Pack JD (1976) Special points for Brillouin-zone integrations. *Physical Review B* 13(12):5188-5192.